SGT

X-622-76-249
PREPRINT

NASA TM X-71234

HIGH SPECTRAL RESOLUTION GROUND-BASED OBSERVATIONS OF VENUS IN THE 450-1250 cm^{-1} REGION

V. G. KUNDE
R. A. HANEL
L. W. HERATH

NOVEMBER, 1976

GSFC — GODDARD SPACE FLIGHT CENTER —
GREENBELT, MARYLAND

X-622-76-249
Preprint

HIGH SPECTRAL RESOLUTION GROUND-BASED OBSERVATIONS OF VENUS IN THE 450-1250 cm^{-1} REGION

V. G. Kunde

R. A. Hanel

L. W. Herath

November, 1976

GODDARD SPACE FLIGHT CENTER

Greenbelt, Maryland

CONTENTS

ILLUSTRATIONS

ILLUSTRATIONS (Continued)

ILLUSTRATIONS (Continued)

TABLES

HIGH SPECTRAL RESOLUTION GROUND-BASED OBSERVATIONS OF VENUS IN THE 450-1250 cm^{-1} REGION

I. INTRODUCTION

The thermal emittance spectrum of a planet contains information on atmospheric temperatures and on gas and particle compositions. The emittance spectrum of Venus has, therefore, been the subject of many observations (Sinton and Strong, 1960; Gillett et al., 1968; Hanel et al., 1968; Moroz et al., 1969; Hanel et al., 1971; Logan et al., 1974; and Ridgway, 1975). In the infrared, ground-based observers are limited to the transmittance windows of the Earth's atmosphere and, therefore, most observations have been carried out in the 750-1250 cm^{-1} range. However, under low humidity conditions at high altitude ground-based observatories additional windows between 400 and 600 cm^{-1} become available. A summary of the salient features of spectroscopic observations of the Venus emittance is shown in Table I. This Table is discussed further in Section VII.

The purpose of this paper is to report on measurements of the emission of Venus recorded during the winter of 1970-1971, and in 1973 using the 2.7m telescope at McDonald Observatory. The double beam Michelson interferometer installed at the Coudé focus was the same instrument used in the 1968 and 1969 measurements of Hanel et al. (1969) except for the detectors (NEP $\sim 5 \times 10^{-13}$ $W \cdot hz^{-1/2}$), the drive system (5 cm mirror excursion), and other minor improvements. The spectrum was recorded between 400 cm^{-1} and 1400 cm^{-1}, although

Table I

Measurements Of The Thermal Emittance Spectrum Of Venus

Investigators	Year of Observation	Resolving Power	Spectral Range (cm^{-1})	Linear Spatial Resolution	Atmospheric Transmission	Calibration	T_m (deg)
Sinton and Strong (1960)	1953, 1954	28-125	769-1250	Full disk	Lunar ratio	Normalized for mean temperature of 225K	239
Gillett et al. (1968)	1967	50	741-3571	Full disk		Broadband stellar network	225
Hanel et al. (1968)	1967	1000	750-1200	Full disk	Direct method	Internal blackbodies	260
Moroz et al. (1969)	1967	80	714-1250	1/30-1/2 disk	Direct method with atmospheric model	Internal blackbody plus narrow band-wide band transfer functions	N/A
Samuelson et al. (1975)	1969	1500	400-1400	1/2 disk	Lunar ratio	Internal blackbodies	228
This Study	1970, 1973	4000-5000	400-1400	1/3-3/4 disk	Lunar ratio	Internal blackbodies	234 (1970) 238 (1973)
Logan et al. (1974)	1974	25	625-2222	Full disk	Direct method with atmospheric model	Cold space from balloon	230
Ridgway (1975)	1975	11000	750-980	1/4 disk	N/A	N/A	N/A

only a part of that interval is transparent enough to extract the Venus emission. For the 1970 observations, the spectral resolution was 0.25 cm^{-1} and the linear spatial resolution was 3/4 of the disk of Venus while in 1973 the spectral resolution was 0.20 cm^{-1} with a spectral resolution 1/3 of the planetary disk. In addition to Venus, the Moon, the sky adjacent to each object, and the zenith sky were recorded to help in the elimination of the absorption and emission effects of the Earth's atmosphere.

The main objective of these observations were to:

(1) explore Venus in the 400-600 cm^{-1} region at high spectral resolution;

(2) obtain adequate spectral resolution and signal-to-noise to positively establish the CO_2 bands in the observed spectral range;

(3) search for spectral features of molecules other than CO_2, particularly in the diffuse 900 cm^{-1} absorption feature;

(4) obtain a radiometrically calibrated thermal emittance spectrum of Venus;

(5) establish the Venus continuum from which information on the cloud opacity and composition is inferred;

(6) use the CO_2 bands to infer information on the thermal structure in the Venus stratosphere.

Objective (5) was discussed recently (Samuelson et al., 1975) using the 1969 observations (Hanel et al., 1971). The 1970 and 1973 measurements discussed in this paper confirm the basic conclusions obtained by Samuelson et al.,

(1975). Objective (6) will be discussed elsewhere. This paper concerns objectives (1) - (4).

II. OBSERVATIONS AND DATA REDUCTION

Venus and the Moon were observed during December, 1970, February, 1971, and December, 1973. These observations were a follow-on to measurements of 0.69 cm^{-1} resolution obtained in April, 1969 with similar instrumentation and the same telescope. Venus was observed in the differential mode in the 1970 session where the sky emittance was cancelled by subtracting optically the planet plus sky emittance in one beam from the adjacent sky emittance in the other beam. For complete cancellation of sky emittance, the optical and electrical characteristics of both paths and detectors must be identical. In practice, some imbalance always remains and the difference spectrum contains residual sky emittance. This residual was minimized by locating Venus alternately in both input beams and adding both sets of Venus spectra. In the 1973 session single beam operation was employed with the planet plus sky and the sky observed sequentially through the same input aperture. The sky emittance was then subtracted from the planetary measurement in the computer. The resulting Venus spectra from both modes of operation were essentially identical.

Generally each source was observed 16 times in succession, the integration time for each interferogram being 97 sec. The signals from the detectors were amplified, band limited, quantized, and stored in digital form on magnetic tape. In the computer, each interferogram was apodized and Fourier transformed into

an uncalibrated power spectrum, and the group of 16 was averaged. The standard deviation among the spectra in a group serves as an indicator of the repeatability and therefore quality of the set. The raw sets of planetary, lunar, and sky spectra were then scaled to spectra obtained in the same way from blackbodies of precisely known temperature. The blackbodies were placed into the optical path between the interferometer and the telescope to calibrate the instrument in an absolute sense. In the case of the downward sky measurements, the blackbodies were placed in front of the sky port located in the ceiling of the Coudé room.

In addition to the radiometric calibration, a small correction in the wave number scale is also applied to the experimental data. The finite and different solid angles of the primary and reference interferometers create a small differential wave number shift. The well-known effect has been corrected for empirically. A numerical fit of a Lorentzian function was made to determine the center wave number position ν_e and ν_t of the strongest CO_2, H_2O, and O_3 features in the observed and in a corresponding synthetic transmittance spectrum, respectively. The adopted correction, $\nu_e - \nu_t$, is shown as a function of ν_t in Figure 1. The adopted correction is a linear least squares fit through the CO_2 lines which are believed to be known more precisely than the water lines,

$$\nu_e - \nu_t = .00024\,\nu_e + .04 . \qquad (1)$$

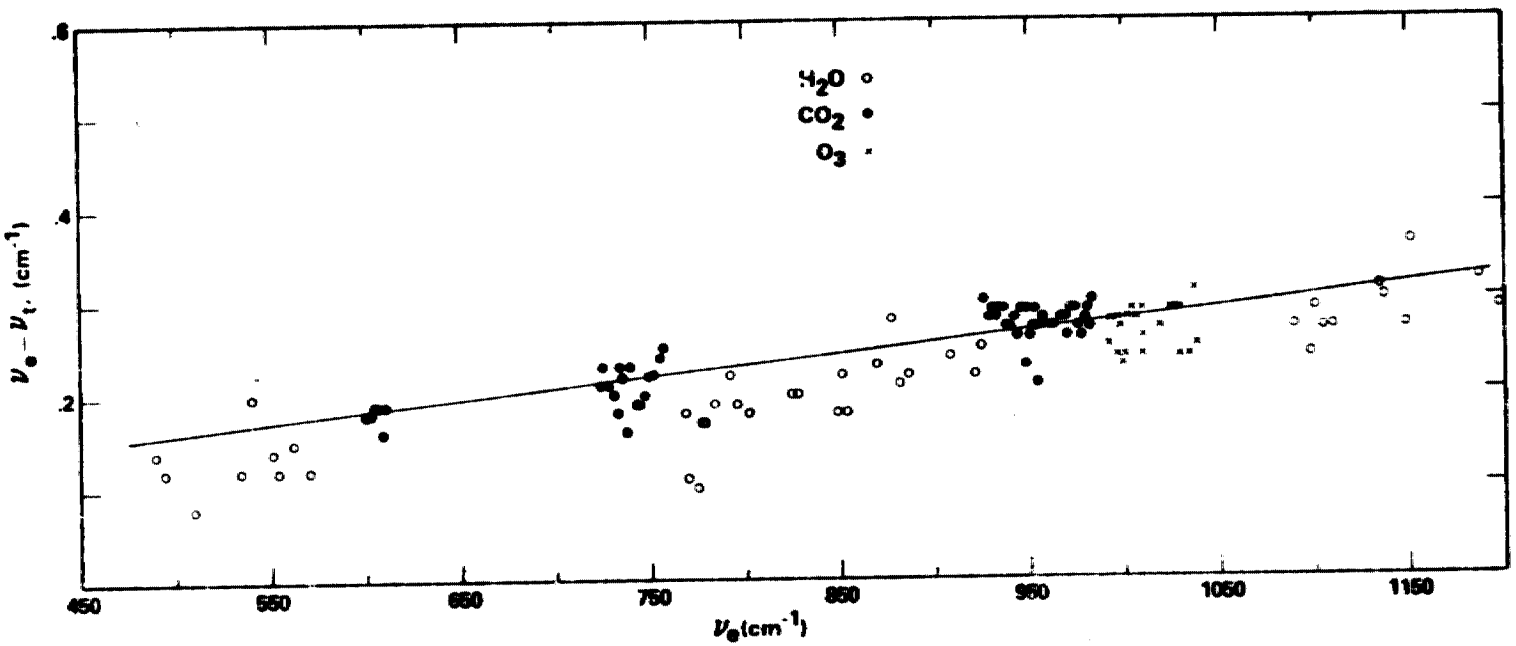

Figure 1. Spectral transfer function to correct experimental wave number scale for finite field of view effects.

After the radiometric and spectral calibration, the next step in the data reduction process — for the single beam Venus observations — is the subtraction of the spectrum recorded while observing the sky through the telescope from the spectrum centered on the object. The telescope is moved approximately two minutes of arc adjacent to Venus or the Moon for the sky only measurement. In the subtraction process, the thermal emittance from the telescope and the Earth's atmosphere is removed. The effect of the atmosphere and telescope transmittance, however, are still present in the resulting difference spectra. The Venus difference spectrum is

$$\bar{I}^{V}_{obs}(\nu) = \bar{I}^{V}(\nu)\, T^{V}_{atm}(\nu)\, T^{V}_{tel}(\nu) \qquad (2)$$

with $\bar{I}^{V}$ the emergent spectrum of Venus and T_{atm} and T_{tel} the transmittance of the terrestrial atmosphere and the telescope, respectively. Both $\bar{I}^{V}_{obs}$ and $\bar{I}^{V}$ represent mean intensities averaged over the field of view. The difference spectrum for double beam operation is given by the same expression. Correspondingly, the measured lunar emittance is

$$\bar{I}^{M}_{obs}(\nu) = \epsilon_s(\nu)\, B(\nu, T_s)\, T^{M}_{atm}(\nu)\, T^{M}_{tel}(\nu) \qquad (3)$$

with ϵ_s the lunar surface emissivity, $B(\nu, T_s)$ the Planck function, and T_s the lunar surface temperature. The differential mode could not be applied to the lunar observations because of the fixed relative position of the two input beams of about 2 minutes of arc.

A best set of difference spectra of Venus and the Moon was then selected from each observing session. Observational parameters for the selected spectra are summarized in Table II with pertinent information of Venus in Table III. The instrument full field of view is θ_I, and the angular diameter of Venus θ_V. With guidance centered on the disk, emission angles from 0^0 to ζ_{max} are included in the observations ($\mu = \cos\zeta$). The fraction of the disk resolved is given by $\sim \theta_I / \theta_V$. The ratio of the apparent areas of the illuminated portion to the entire is k, and the phase angle is i.

Table II

Observational Parameters

Date	Local Time (Hr : Min.)	Object	Zenith Angle (Deg.)	Air Mass
December 16, 1970	11:48	Venus	~51	1.59
February 16, 1971	3:50	Moon	~51	1.59
December 20, 1973	15:00	Venus	~51	1.60
December 17, 1973	8:55	Moon	~44	1.40

Table III

Venus Characteristics

Date	θ_I (arc. sec.)	θ_v (arc. sec.)	θ_I/θ_v	ζ_{max} (deg.)	μ_m	k	i (deg.)
December 16, 1970	30.6	40.5	.76	49.1	.65	.266	118.0
December 20, 1973	16.0	44.3	.36	21.2	.93	.246	120.5

III. TELESCOPE AND ATMOSPHERE TRANSMITTANCE

The Venus spectrum may be determined in absolute radiometric units by a direct method or by ratioing to the observed lunar spectrum. In the direct method, experimental or theoretical knowledge of the atmospheric and telescopic transmittance functions is needed to remove their effects from the Venus observations. In the ratio technique, those effects are removed by cancellation. The ratio method has the added advantage that systematic instrument factors tend to cancel. The determination of the telescopic and atmospheric transmittance functions for the direct method is discussed below.

The telescope transmittance function was derived from an analysis of weak molecular atmospheric lines in the downward sky emittance measured with and without the telescope. Another technique using the continuum portion of the spectrum was also used, with results very similar to the weak line technique. The telescope transmittance, shown in Figure 2, includes losses due to the reflectances of the five telescope mirrors and obscuration by elements in the telescope, mainly the secondary mirror and its supporting spider. The method of estimating the telescope transmittance is fairly reliable between 750 cm^{-1} and 950 cm^{-1}, where many weak water vapor lines are available for analysis, but is less reliable towards the more strongly absorbing parts of the spectrum. As a result, only a first order linear spectral dependence has been assumed for the telescope transmittance even though some nonlinearity is expected from the overlying dust particles and overcoating materials on the mirrors.

Thus, the normalization procedure was necessary to remove the above broad scale uncertainties from the atmospheric transmittance spectrum. Using the low resolution ϵ_s, the atmospheric transmittance was then computed at full resolution (0.25 cm^{-1}) according to Equation (4). The resulting transmittances are shown as the upper curves in Figures 3 and 4. The general agreement of the overall level of the observed and synthetic spectra is, therefore, forced by the procedure. However, the agreement of details with scales smaller than 20 cm^{-1} is not affected by this empirical elimination of the effects of the telescope transmittance and lunar emissivity.

The synthetic atmospheric transmittance spectrum assumes the mid-latitude winter model from McClatchey et al. (1970) for the atmospheric temperature profile. The volume mixing ratios adopted are illustrated in Figure 5. The distributions for the variable gases H_2O and O_3 were obtained by uniformly scaling the mid-latitude winter vertical distributions until the synthetic and experimental spectra matched in terms of band contour for the 1042 cm^{-1} band of O_3 and line depths for H_2O in the 750-1250 cm^{-1} region. The scaled gas distributions correspond to total vertical columnar gas abundances of .31 pr cm H_2O and .30 cm atm O_3. The radiative transfer equation was solved numerically, using a direct integration technique (Kunde and Maguire, 1974), with the molecular parameters (CO_2, H_2O, N_2O, O_3, CH_4) adopted from the AFCRL compilation (McClatchey et al., 1973).

For the direct method, the terrestrial atmospheric absorption was removed from the Venus spectrum with a theoretical slant path line by line transmittance model (Kunde and Maguire, 1974). To establish confidence in the model, the atmospheric transmittance was derived from the lunar spectrum and compared to a theoretical spectrum synthesized on a computer. The observed atmospheric transmittance was calculated from Equation (3)

$$T_{atm}(\nu) = \overline{I}^{M}_{obs}(\nu) / \epsilon_s(\nu)\, B(\nu, T_s)\, T^{M}_{tel}(\nu) . \qquad (4)$$

The lunar surface temperature was derived at 900 cm^{-1} by assuming a 0.99 transmittance of the atmosphere at that wave number and the appropriate telescope transmittance ($\sim .57$). Furthermore, a lunar emissivity of unity was assumed for that wave number. The resulting lunar surface temperature for the subsolar point was found to be 393K, which compares favorably to 385K derived from the thermal maps of Montgomery, et al. (1966). The observed lunar spectrum was then normalized at low resolution (~ 50 cm^{-1}) to the theoretical transmittance to derive an empirical function for the lunar emissivity. The telescope transmittance used was the linear representation of Figure 2. The comparison was made at low resolution, as ϵ_s is not expected to change rapidly with wave number. The derived ϵ_s function only partially resembled the expected weak silicate reststrahlen spectrum. Significant contamination from other possible sources, such as inadequate modeling of the theoretical H_2O continuum absorption and/or small scale non-linear telescope transmission features, was present.

Thus, the normalization procedure was necessary to remove the above broad scale uncertainties from the atmospheric transmittance spectrum. Using the low resolution ϵ_s, the atmospheric transmittance was then computed at full resolution (0.25 cm^{-1}) according to Equation (4). The resulting transmittances are shown as the upper curves in Figures 3 and 4. The general agreement of the overall level of the observed and synthetic spectra is, therefore, forced by the procedure. However, the agreement of details with scales smaller than 20 cm^{-1} is not affected by this empirical elimination of the effects of the telescope transmittance and lunar emissivity.

The synthetic atmospheric transmittance spectrum assumes the mid-latitude winter model from McClatchey et al. (1970) for the atmospheric temperature profile. The volume mixing ratios adopted are illustrated in Figure 5. The distributions for the variable gases H_2O and O_3 were obtained by uniformly scaling the mid-latitude winter vertical distributions until the synthetic and experimental spectra matched in terms of band contour for the 1042 cm^{-1} band of O_3 and line depths for H_2O in the 750-1250 cm^{-1} region. The scaled gas distributions correspond to total vertical columnar gas abundances of .31 pr cm H_2O and .30 cm atm O_3. The radiative transfer equation was solved numerically, using a direct integration technique (Kunde and Maguire, 1974), with the molecular parameters (CO_2, H_2O, N_2O, O_3, CH_4) adopted from the AFCRL compilation (McClatchey et al., 1973).

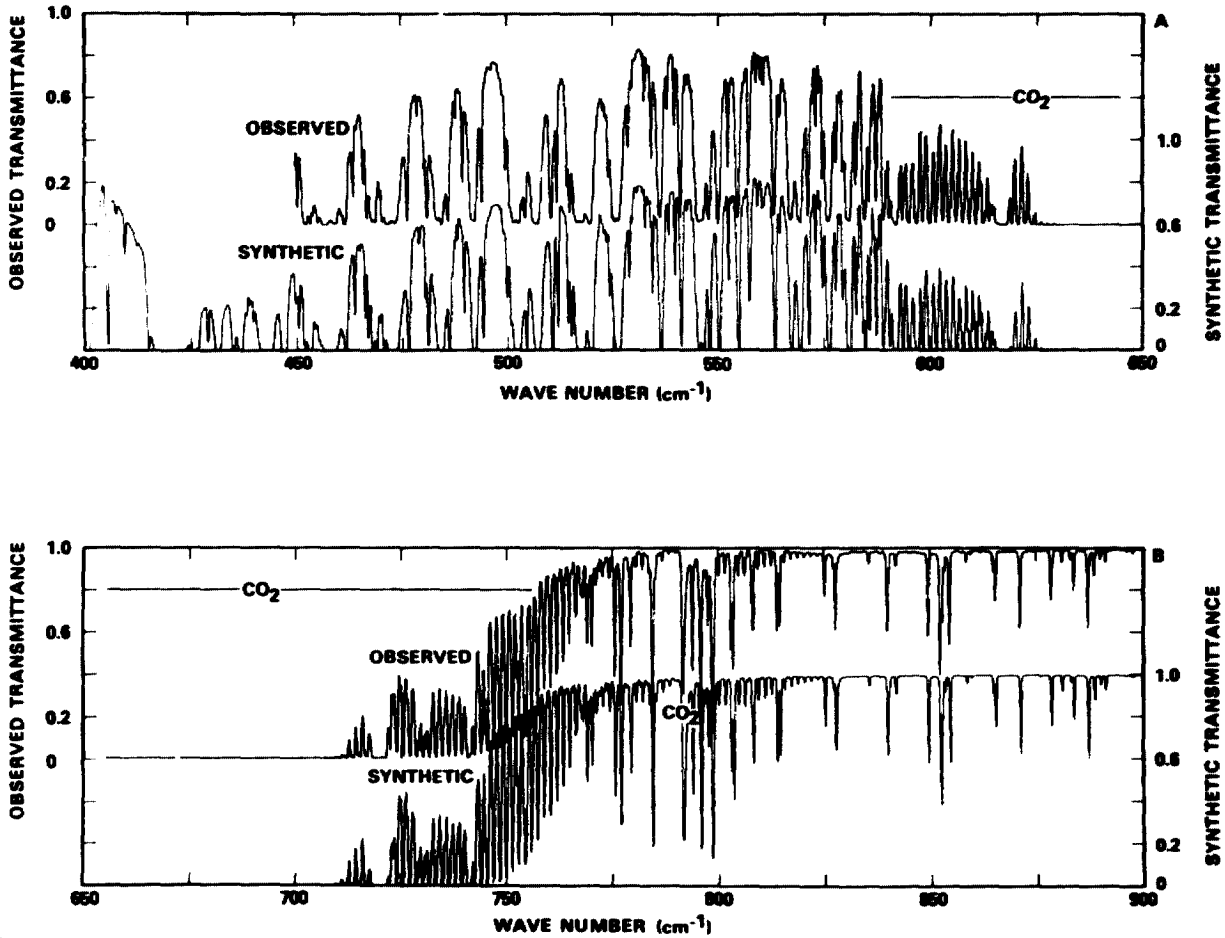

Figure 3. A, B. Atmospheric transmittance at 0.25 cm^{-1} resolution for the 400–650 and 650–900 cm^{-1} regions derived from observations of the moon. Numerous spectral lines are resolved for absorption bands of H_2O and CO_2. A synthetic comparison spectrum is also shown.

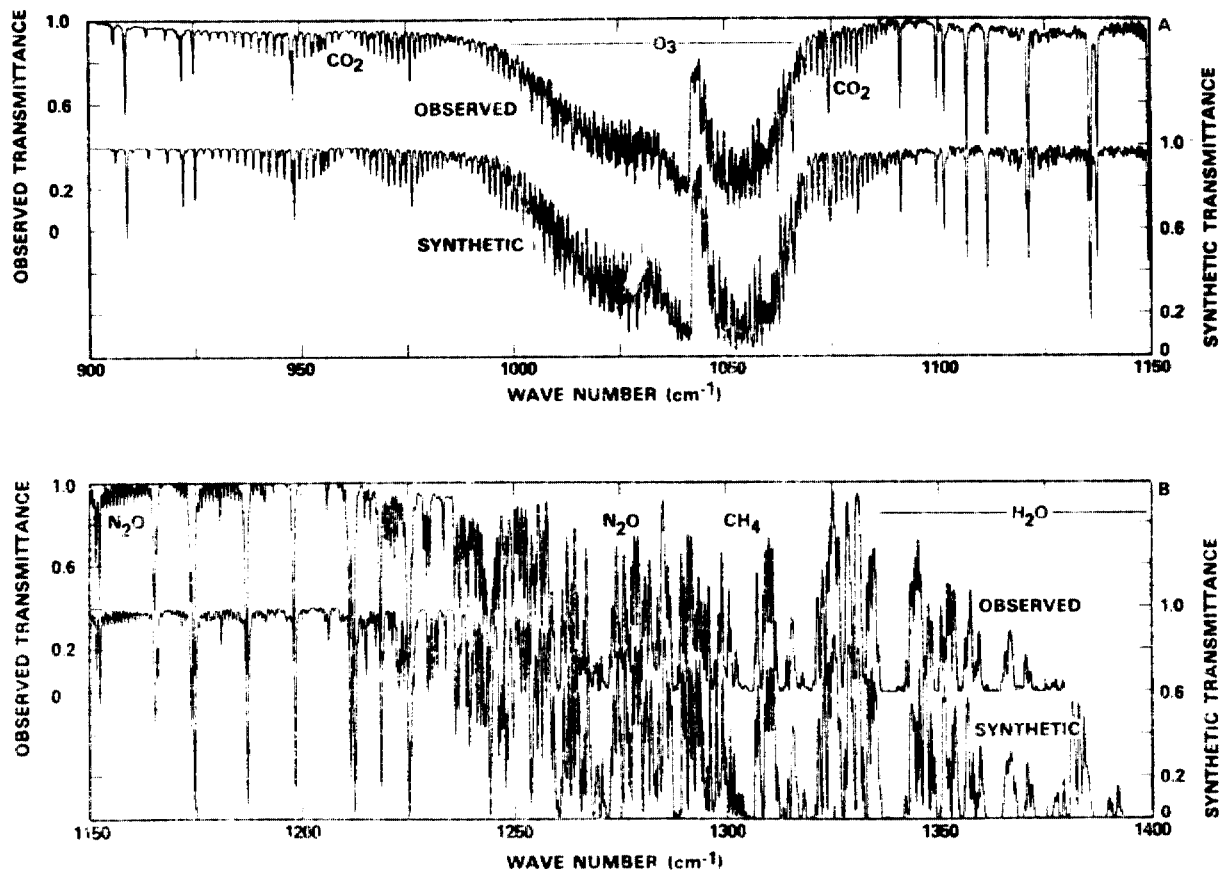

Figure 4. A, B. Atmospheric transmittance at 0.25 cm^{-1} resolution for the 900-1150 and 1150-1400 cm^{-1} regions derived from observations of the moon. Numerous spectral lines are resolved for absorption bands of CO_2, O_3, H_2O, N_2O and CH_4. A synthetic comparison spectrum is also shown.

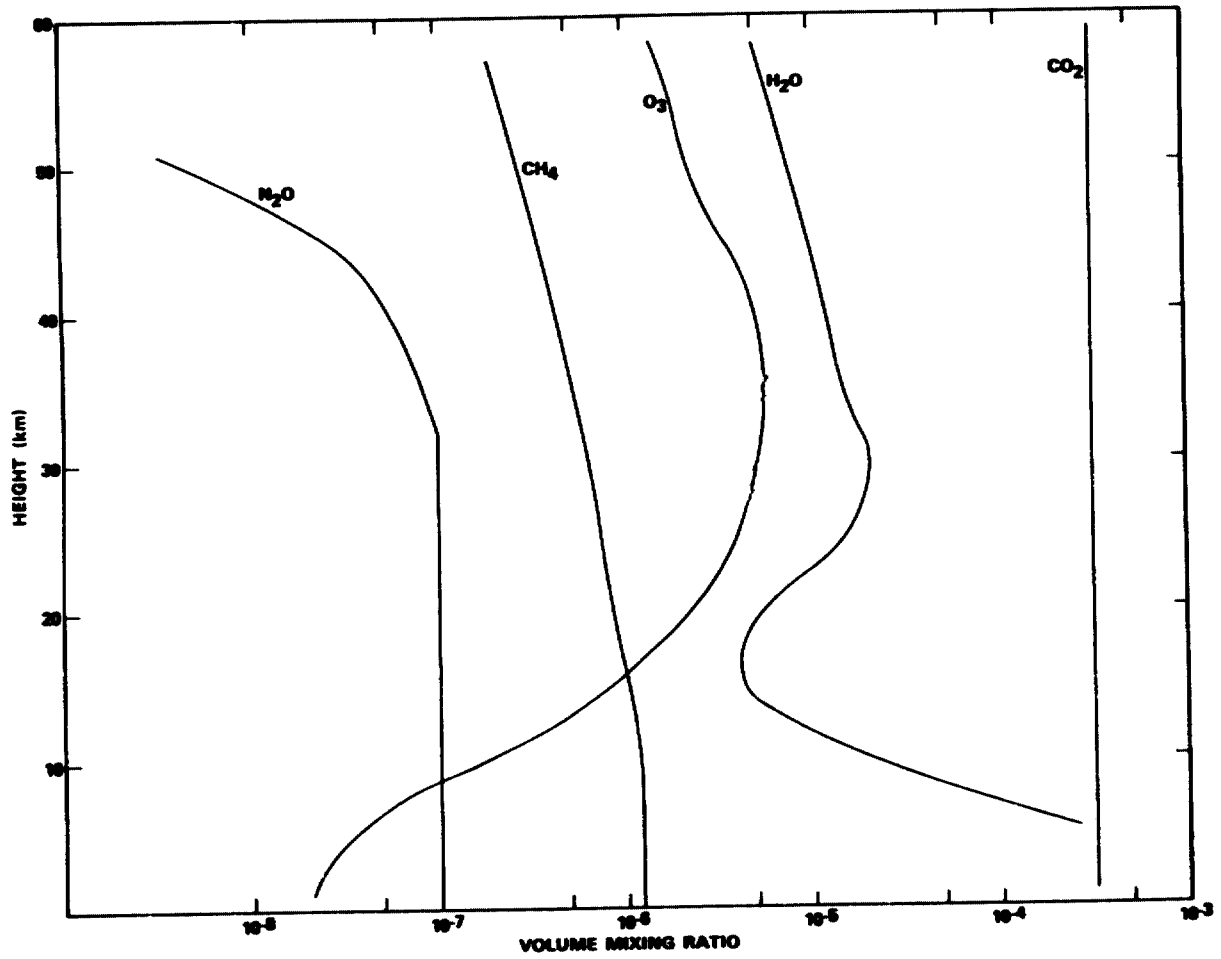

Figure 5. Volume mixing ratios adopted for model atmosphere used to generate synthetic atmospheric transmittance.

Agreement between the observed and synthetic spectra indicates that the gases included in the computation account fairly well for the atmospheric transmittances. However, some quantitative disagreement is apparent between 1150 cm^{-1} and 1200 cm^{-1} where the measured N_2O lines are apparently much stronger than the synthetic counterparts.

Due to the above uncertainties in the empirical telescope and lunar emissivity functions, and in the continuum absorption of the theoretical transmittance model, the direct method was not used for the derivation of the final Venus spectra. Instead, the ratio technique was adopted with the moon used as an intermediate calibration object.

IV. DOWNWARD SKY EMITTANCE

In contrast to the atmospheric transmittance, which has to be derived from the lunar spectra assuming knowledge of the lunar surface emissivity as well as of the telescope transmittance, the atmospheric emittance can be measured directly. The purpose of this direct measurement was to help in the estimation of telescope transmittance and at the same time give an additional check on the atmospheric transmittance model. The same molecular parameters which determine the transmittance appear in the synthetic emittance spectrum.

The sky radiation entered the Coudé room through an overhead port and was channeled to the interferometer via a flat mirror mounted on the telescope turret. The telescope optical train is bypassed, and effects due to the transmission and emission of the telescope are, therefore, not present in this

measurement. An example of the downward sky emittance obtained on February 17, 1971 is presented in Figures 6 and 7. Gas lines seen in transmission in Figures 3 and 4 may now be seen in emission. The downward monochromatic radiation is

$$I(\nu) = \int_{1}^{T_{min}} B(\nu, T(T))\, d\, T(\nu) \qquad (5)$$

where T is the monochromatic transmittance between a given atmospheric level and the bottom of the atmosphere. The atmospheric emittances are summed from the bottom of the atmosphere ($T = 1$) to the top of the atmosphere ($T = T_{min}$). The theoretical downward monochromatic emittance has been computed and convolved with an instrument function corresponding to $\Delta\nu = 0.25\ cm^{-1}$. The synthetic downward sky emittance spectrum is also presented in Figures 6 and 7. The mid-latitude winter model, discussed in the transmittance section, again served in the computation of the synthetic sky emittance. The temperature and water vapor profiles were scaled and normalized to surface values measured at McDonald Observatory. The comparison shows general agreement throughout the measured spectral range. Emission from strongly absorbing regions, such as the peaks of the strong CO_2 and H_2O lines, originates along the optical path in the Coudé room. As the temperature gradient along this path varies from that of the lower portion of the atmospheric model, valid comparisons may not be made in strongly absorbing parts of the spectrum, such as in the 600-700 cm^{-1} region of CO_2.

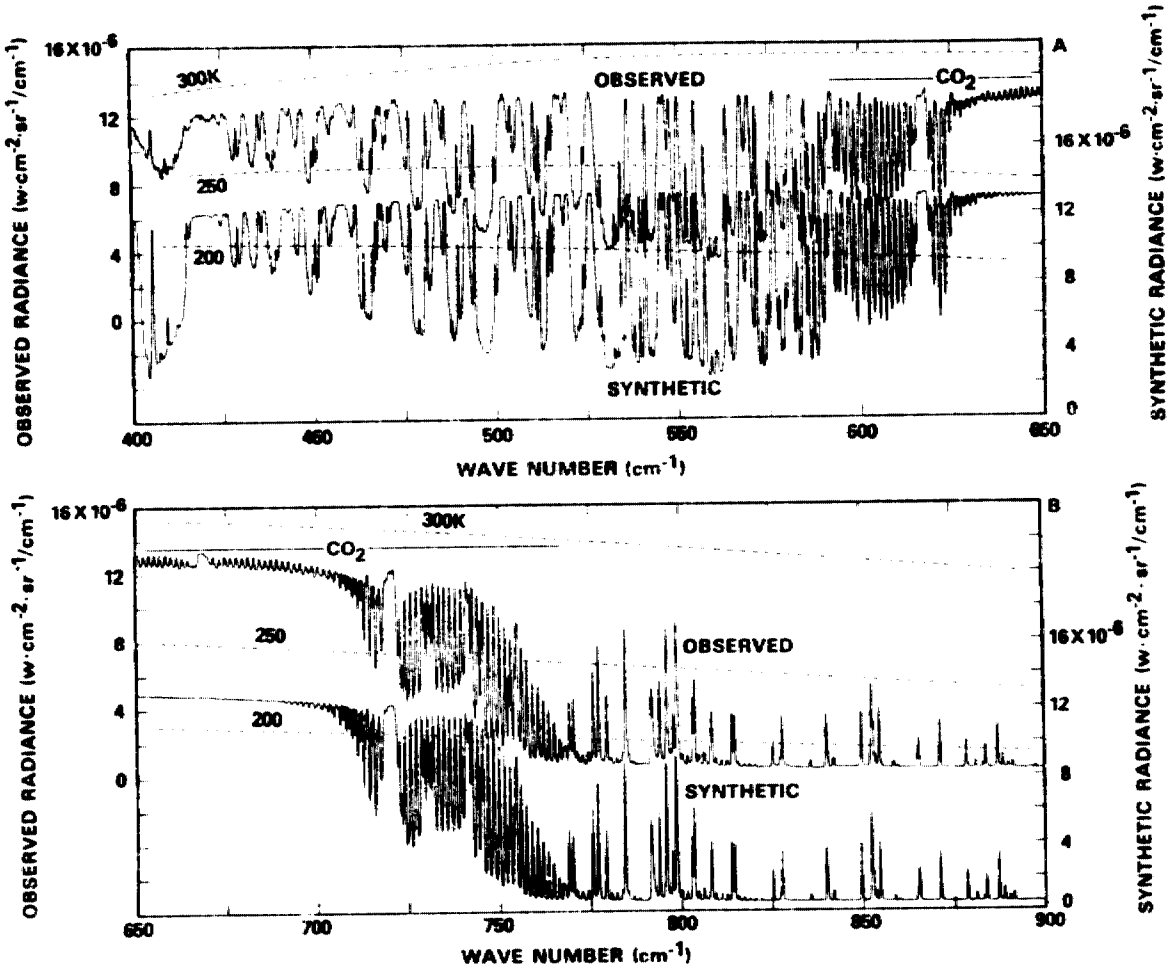

Figure 6. A, B. Downward zenith sky emittance at 0.25 cm^{-1} resolution for the 400–650 and 650–900 cm^{-1} regions. Numerous spectral lines are resolved for absorption bands of H_2O and CO_2. A synthetic comparison spectrum is also shown.

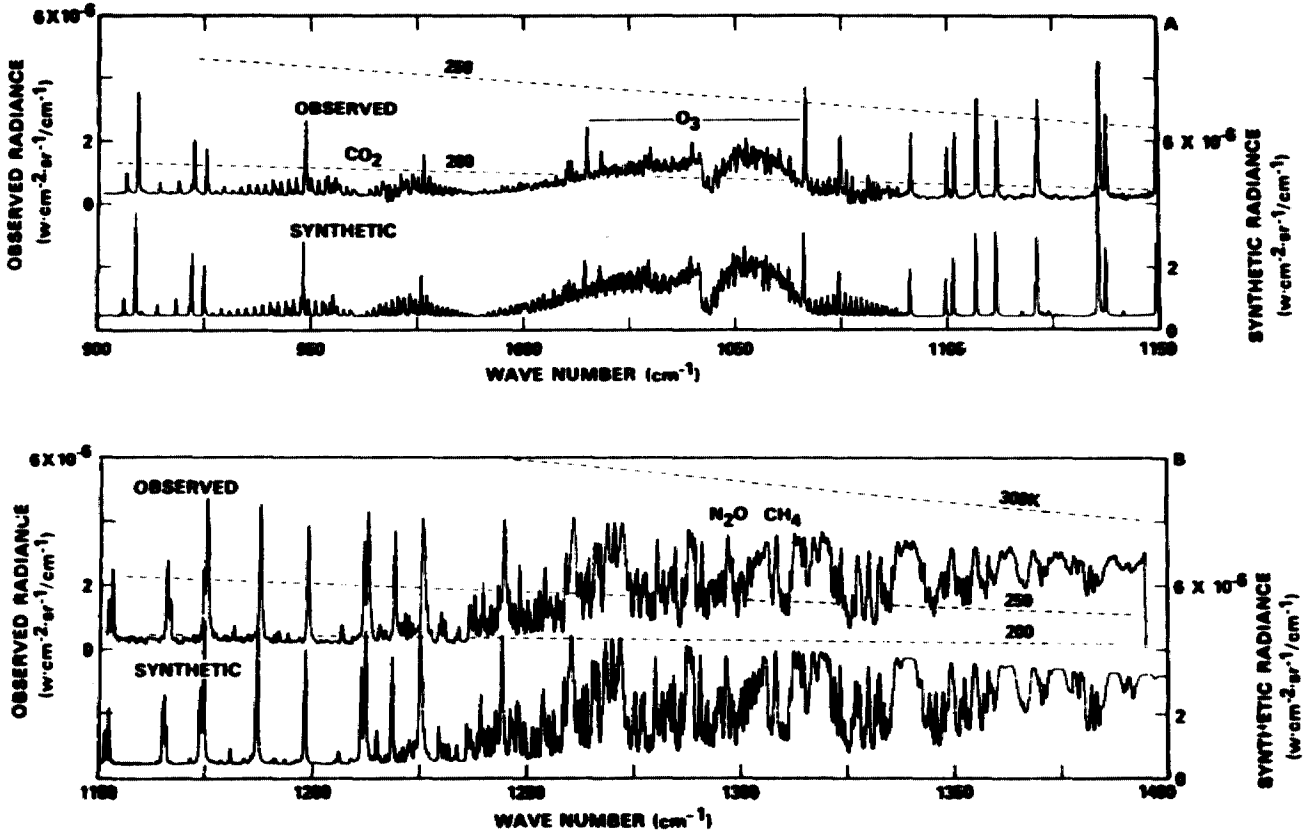

Figure 7. A, B. Downward zenith sky emittance at 0.25 cm^{-1} resolution for the 900–1150 and 1150–1400 cm^{-1} regions. Numerous spectral lines are resolved from absorption bands of CO_2, O_3, H_2O, N_2O and CH_4. A synthetic comparison spectrum is also shown.

Emission from H_2O lines may be seen throughout the observed spectral range. The pure rotational transitions occur in the 425-1000 cm^{-1} region with the stronger transitions being near the 425 cm^{-1} observational limit. As with the transmittance comparison, the synthetic H_2O absorption continuum appears too transparent. Strong H_2O emission by the P-branch lines of the 1595 cm^{-1} ν_2 band may be seen in the 1200-1400 cm^{-1} region. The strong ν_2 fundamental of CO_2 is mainly responsible for the emission in the 550-775 cm^{-1} region with additional features due to bands at 618, 721, 742, 757 and 791 cm^{-1}. Other upper state CO_2 bands occur at 961 and 1064 cm^{-1}. The ν_3 fundamental of O_3 dominates between 1000 and 1070 cm^{-1} and the ν_4 fundamental of CH_4 at 1306 cm^{-1}. Bands of N_2O occur in the 1285 cm^{-1} region.

V. VENUS MODEL ATMOSPHERE

To correspond to the observed difference spectrum, the theoretical emergent spectrum is averaged over the instrumental field of view

$$\bar{I}(\nu, \mu_M) = \int_{\mu_M}^{1} I(\nu, \mu)\, \mu d\mu \Big/ \int_{\mu_M}^{1} \mu d\mu \qquad (6)$$

where $I(\nu, \mu)$ is the specific intensity for $\mu = \cos \zeta$. The intensity $I(\nu, \mu)$ has been assumed to be independent of position on the planet. The maximum direction cosines and the corresponding emission angles for the 1970 and 1973 observations are given in Table III. For full disk measurements $\mu_M = 0$, corresponding to a maximum emission angle of 90°.

Because of limb darkening, the observed spectrum is dependent on the instrumental field-of-view. For scientific analysis and for intercomparison of observational data sets, it is beneficial to remove the limb darkening and present the observations in terms of a more common and instrument-independent physical parameter. The specific intensity in the vertical at the center of the disk, $I(\nu,1)$, has been chosen for this investigation. Model atmosphere calculations have been used to correct the observations for limb darkening. Synthetic spectra at the instrumental resolution were computed for $I(\nu,1)$ and $\bar{I}(\nu, \mu_M)$ with a scaling factor

$$F(\nu, \mu_M) = I(\nu, 1) / \bar{I}(\nu, \mu_M) \qquad (7)$$

derived from the ratio of the spectra. This scaling factor was then used to numerically remove the limb darkening from the measured difference spectrum. The corrections are small, the maximum values being 6 and 1% for the 1970 and 1973 observations, respectively. The model includes aerosol, and gaseous CO_2 and H_2O absorption. The temperature profile of Venus was inverted from the 791 cm^{-1} CO_2 band and is close in absolute value to the stratospheric temperature profile from the Mariner 9 occulation experiment (Fjeldbo, et al., 1971).

The haze cloud layer in the 100-300 mb region of the Venus atmosphere represents the lower boundary for the radiation in the 400-1400 cm^{-1} region.

This layer is currently assumed to consist of an aqueous solution of sulfuric acid with the H_2SO_4 concentration by weight in the 75-85% range (Samuelson et al., 1975; Pollack et al., 1976). A 75% concentration was adopted for this calculation, with the extinction across-sections computed from the optical constants of Pinkley et al., (1976) at 250 K. The aerosol was assumed to be homogeneously mixed with the gaseous atmosphere.

The above model and the limb darkening will be discussed elsewhere.

VI. VENUS THERMAL EMITTANCE SPECTRUM

As discussed in Section III, the ratio technique was adopted for the derivation of the final Venus spectra. From (2) and (3), the Venus spectrum relative to the Moon is

$$\bar{I}^{V}_{(\nu)} = \left[\frac{\bar{I}^{V}_{obs}(\nu)}{\bar{I}^{M}_{obs}(\nu)}\right] \Delta T_{cor} \epsilon_s(\nu)\, B(\nu, T_s). \qquad (8)$$

The telescope transmittance has been assumed equal for both measurements. For the 1970-1971 session the Venus and lunar measurements were obtained under nearly identical geometrical observing conditions. As a result, transmittance effects due to constantly mixed gases in the Earth's atmosphere will cancel. This assumption is not completely satisfied for the variably mixed gases (H_2O, O_3) because of the large temporal difference (December vs February) in the Venus and lunar observations. The Venus ratio spectrum thus contains small residual terrestrial line features of H_2O and O_3, represented by

ΔT_{cor} in Equation (8). These features have been removed with a theoretical atmospheric slant path transmittance program by varying the H_2O and O_3 gas concentrations until the residual lines were minimized. This correction is significant to the interpretation of the spectrum only in the 1000–1100 cm^{-1} region of ozone absorption. The most closely matched lunar-Venus spectra for the 1973 session yielded a Venus ratio spectrum still containing atmospheric effects corresponding to a residual air mass of 0.2. This ΔT_{cor} correction was also determined theoretically. The ratio spectrum was computed only for spectral regions where the atmospheric transmission is greater than 0.2.

Uncertainties in the Venus spectrum arise from inadequate knowledge of the emissivity and temperature of the lunar surface. The lunar emissivity was assumed to be unity for this study. The effects of the lunar emissivity on the Venus spectrum were illustrated in Samuelson et al., (1975), where it was concluded that these features did not significantly affect the major conclusions concerning the Venus spectrum. The resulting expression for the observed Venus spectrum is now

$$\bar{I}^V(\nu) = \left[\frac{\bar{I}^V_{obs}(\nu)}{\bar{I}^M_{obs}(\nu)}\right] B(\nu, T_s) \qquad (9)$$

The surface temperature of the moon was derived internally from the lunar measurement in the 900 cm^{-1} region in the manner described in the previous section. The observed mean intensity computed from Equation (9) was transformed to the central intensity in the vertical ($I(\nu,1)$) as described in Section V.

The derived vertical intensities are presented in terms of brightness temperature for the 450-1250 cm^{-1} region in Figure 8 and also on an expanded scale in Figures 9, 10, and 11. The accompanying synthetic spectrum was computed with the Venus model described in Section V and is shown to assist in the spectral and gross quantitative comparisons. A more refined description of the thermal structure and aerosol characteristics is necessary for a detailed quantitative comparison. The spectral gaps in the 600-750 cm^{-1} and 1030-1075 cm^{-1} ranges are a result of absorption by terrestrial CO_2 and O_3, respectively. The high spectral resolution allows information on the Venus spectrum to be obtained in the narrow windows between the strong terrestrial lines. Thus, the Venus spectrum may be partially obtained from 525-605 and 755-800 cm^{-1}, regions not accessible with low spectral resolution. The transparency of the atmosphere near 1042 cm^{-1}, between the P and R branches of the ν_2 O_3 fundamental, allows identification of several rotational lines of the 1064 cm^{-1} band of CO_2 to be made in this region of the Venus spectrum.

Effects due to CO_2 absorption can be seen throughout most of the spectral range. The large decrease in brightness temperature in the 550-600 and 750-800 cm^{-1} regions is mainly due to the strong absorption of P and R branch lines of the CO_2 ν_2 fundamental at 667 cm^{-1}.

Other CO_2 bands with weak spectral features have been identified in the spectrum and are listed in Table IV. The five distant narrow features in the 450-550 cm^{-1} region are due to the CO_2 bands at 471 and 508 cm^{-1}. The mean

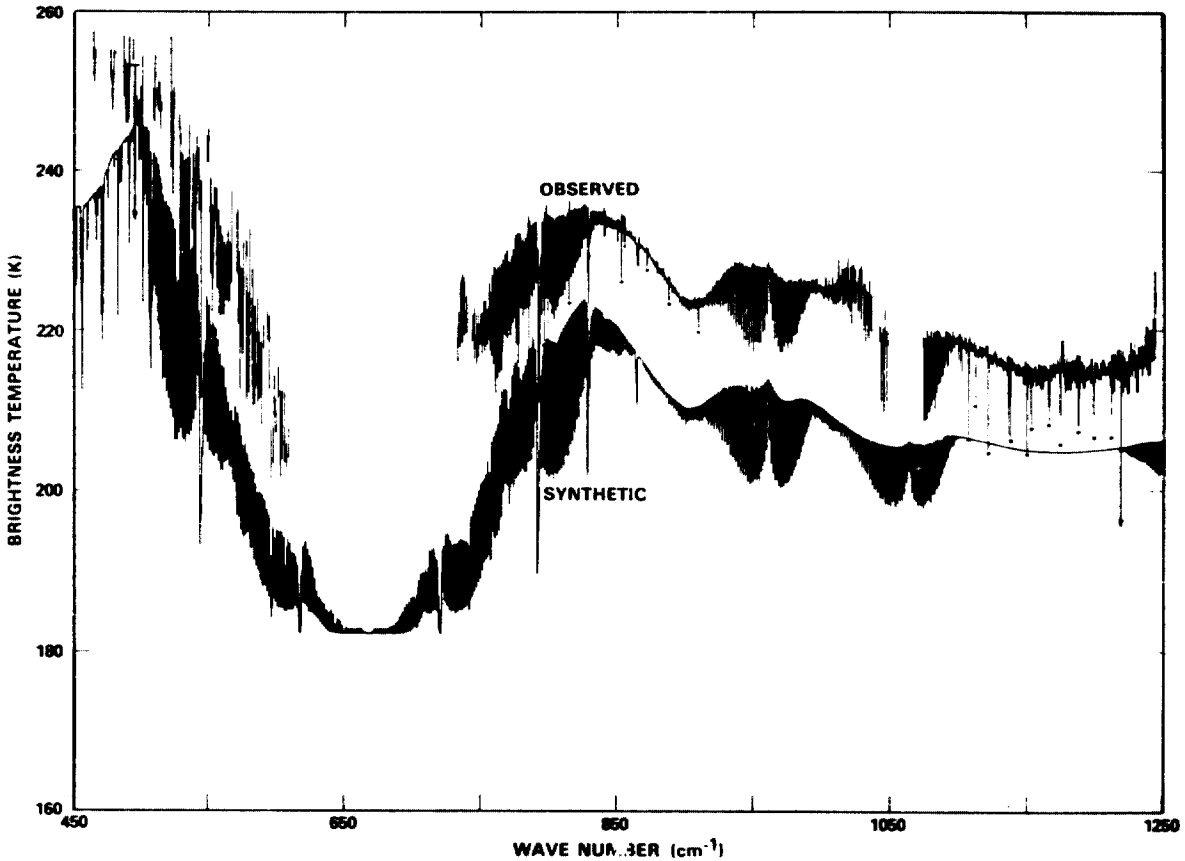

Figure 8. Venus thermal emittance spectrum in the 450-1250 cm^{-1} region at 0.25 cm^{-1} resolution obtained from McDonald Observatory in December 1970. A limb-darkening correction has been applied and the brightness temperatures correspond to the emergent radiance in the vertical. The integration time was ~ 52 minutes. The lines marked with an asterisk are residual terrestrial absorption lines which have not been completely compensated for by the correction techniques used. The residual effect is only important in the local region of the absorption line. The synthetic comparison spectrum has been displaced 20K vertically downward for clarity of presentation. The vertical arrows indicate this offset from the observed spectrum.

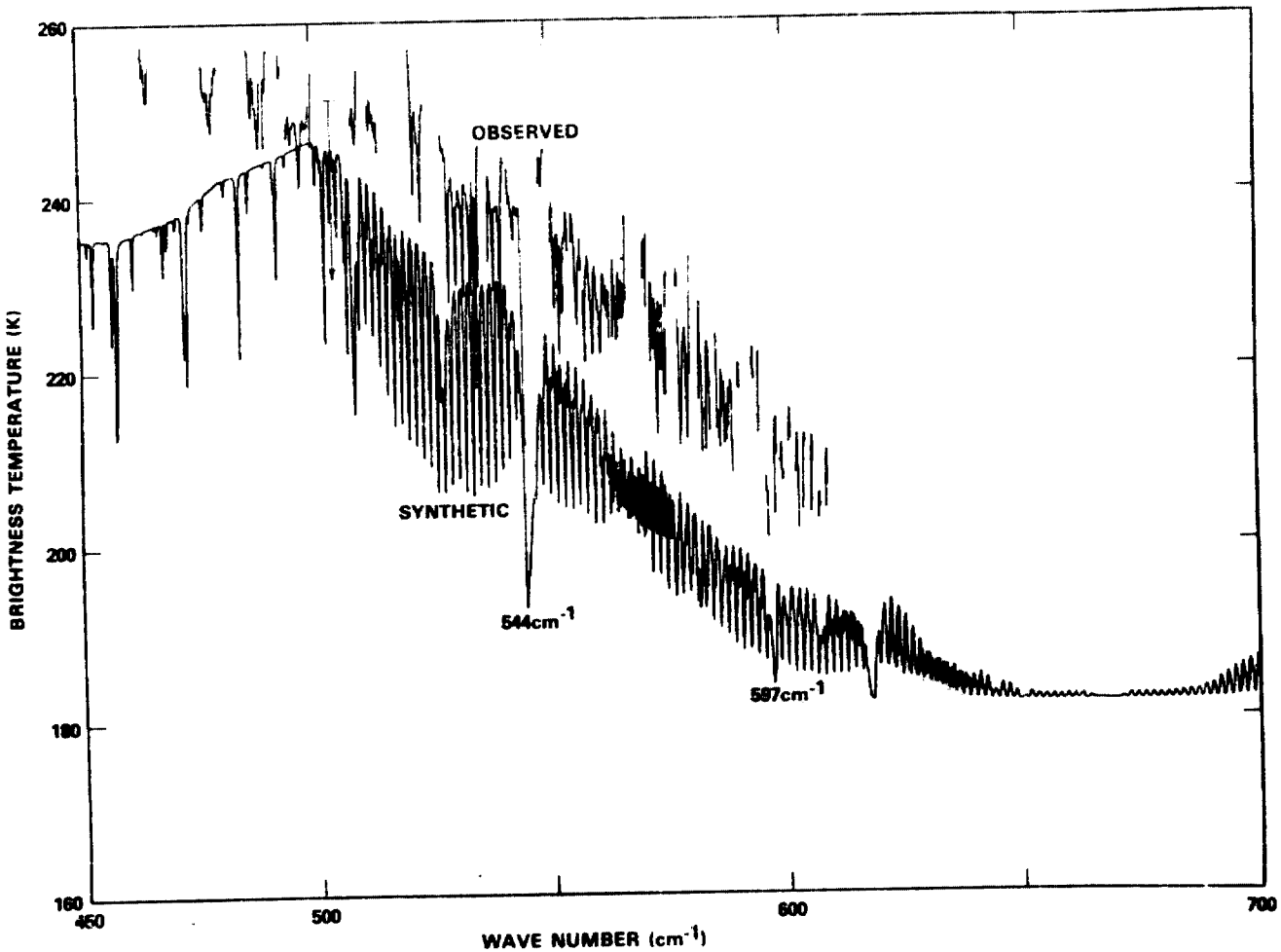

Figure 9. Same as Figure 8, except for 450-700 cm^{-1} region. Numerous CO_2 vibration-rotation absorption lines are evident, including the five distinct lines in the 450-500 cm^{-1} region. The lines in the 450-500 cm^{-1} range of the synthetic spectrum are due to Venusian H_2O. In the observed spectrum these lines have been blocked out by terrestrial H_2O.

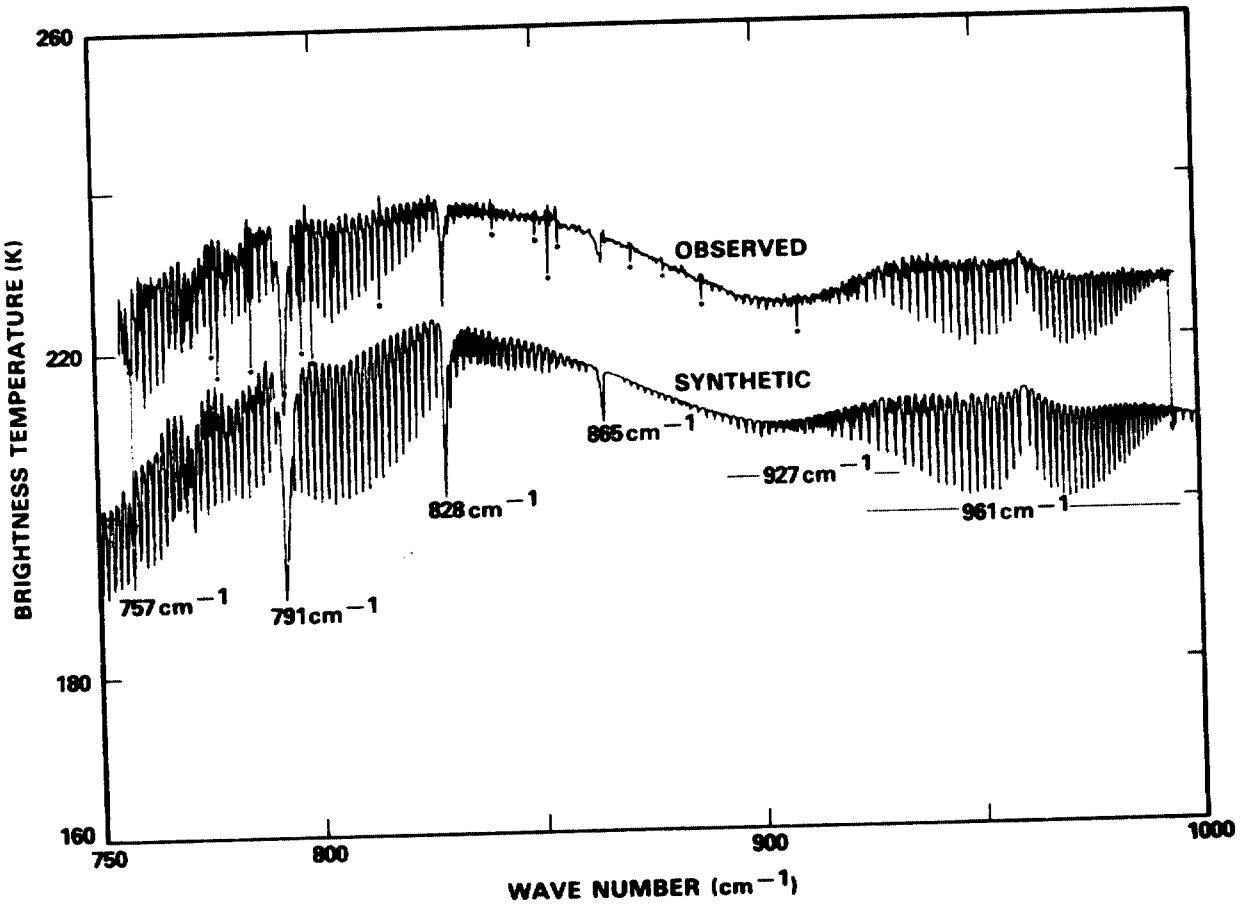

Figure 10. Same as Figure 8, except for 750-1000 cm^{-1} region. Numerous CO_2 vibration-rotation absorption lines are evident. The broad absorption feature in the 900 cm^{-1} region is associated with the sulfuric acid haze. The lines in this feature are due to the 927 cm^{-1} CO_2 band.

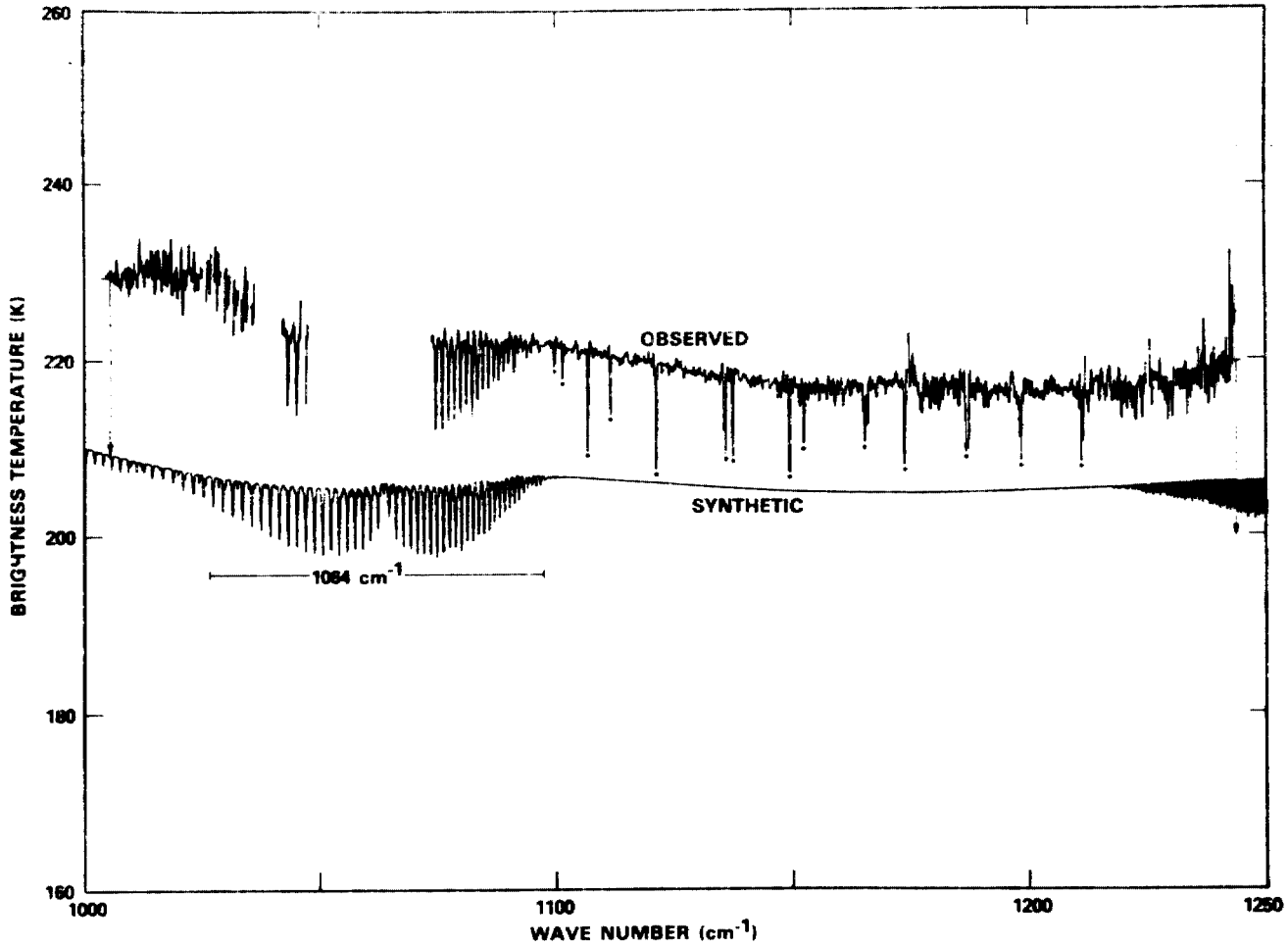

Figure 11. Same as Figure 8, except for 1000–1250 cm^{-1} region. The only CO_2 band identified in the Venus spectrum in this region is at 1064 cm^{-1} .

Table IV

Weak CO_2 Bands Observed in the Venus Thermal Emission Spectrum

ν_0 (cm^{-1})	Vibrational Quantum Numbers		E (cm^{-1})	Type	S ($mol^{-2} \cdot cm^2 \cdot cm^{-1}$)
	Upper State $v_1\ v_2\ \ell\ v_3\ r$	Lower State $v_1\ v_2\ \ell\ v_3\ r$			
471.41	20003	11101	2076.86	$\Sigma - \Pi$	8.70×10^{-25}
508.14	12202	11101	2076.86	$\Delta - \Pi$	5.16×10^{-24}
544.28	11102	10001	1388.19	$\Pi - \Sigma$	3.76×10^{-22}
597.34	11102	02201	1335.13	$\Pi - \Delta$	5.58×10^{-21}
757.50	12201	03301	2003.24	$\Delta - \Phi$	2.17×10^{-22}
791.45	11101	10002	1285.41	$\Pi - \Sigma$	8.32×10^{-22}
828.26	12201	11102	1932.47	$\Delta - \Pi$	2.54×10^{-23}
864.68	20001	11102	1932.47	$\Sigma - \Pi$	4.32×10^{-24}
927.15	01111	11101	2076.86	$\Pi - \Pi$	3.56×10^{-23}
960.96	00011	10001	1388.19	$\Sigma - \Sigma$	6.27×10^{-22}
1063.73	00011	10002	1285.41	$\Sigma - \Sigma$	1.03×10^{-21}

spacing of P and R branch lines of the observed CO_2 bands depends strongly on the value of the vibrational angular momentum about the internuclear axis (ℓ), the standard designation for $\ell = 0, 1, 2, 3, \ldots$ being Σ, Π, Δ, Φ. . . Only even J rotational lines, corresponding to transitions between symmetric rotational levels, exist for the $\Pi - \Sigma$ and $\Sigma - \Sigma$ bands with a mean line spacing

of $\sim$ 1.6 cm^{-1}. The nuclear spin statistics for CO_2 do not permit antisymmetric levels to exist, and transitions from these levels (odd J) in the ground state are forbidden. The P and R branches of the bands at 791, 961, and 1064 cm^{-1} are classic examples of $\Pi - \Sigma$ and $\Sigma - \Sigma$ transitions. For the Π, Δ and Φ states, the ℓ-type doubling gives symmetric and antisymmetric levels for each rotational J state. For $\Delta - \Phi$, $\Pi - \Delta$, and $\Pi - \Pi$ bands, each J transition consists of two components, one from the symmetric levels and the other from the asymmetric levels. Again, CO_2 nuclear spin statistics forbid the asymmetric level transitions. The appearance of these bands consists of the staggering of P and R branch lines (Herzberg, 1945) with altering line spacing of $\sim$ 0.5 and $\sim$ 1.0 cm^{-1}. The P and R branches of the bands at 758, 828, and 927 cm^{-1} exhibit this structure. The rotational structure of all the observed molecular bands is well developed at the 0.25 cm^{-1} resolution of the observed spectra. As expected, no water vapor absorption lines were seen on Venus due to the strong terrestrial H_2O absorption.

A visual search of the measured spectrum was made for features due to suspected trace constituents, such as H_2S, COS, etc. No spectral features due to other atomic or molecular species, besides CO_2, were found. All statistically significant sharp line absorption features have been identified with gaseous CO_2.

Five prominent diffuse spectral features in the 450, 580, 900, 1050 and 1165 cm^{-1} regions characterize the infrared spectrum of the aqueous H_2SO_4

haze. In these regions, good agreement is found between the observed and synthetic spectra, with the exception of the 450 cm^{-1} feature which does not appear to be present in the observed spectrum. However, additional observations and more complete spectral coverage is required in this region for confirmation. Additionally, aerosol modeling effects, such as temperature dependence of the optical constants, size distribution of the cloud droplets, etc., unique to this spectral region must be further investigated. No indication of the 580 cm^{-1} H_2SO_4 feature is seen in the observed spectrum. This is expected, however, as the strong CO_2 absorption in this region would dominate the H_2SO_4 absorption. The general shape of the observed spectrum in the 500-600 cm^{-1} region agrees well with that of CO_2 only. The 900 cm^{-1} H_2SO_4 band is associated with the broad diffuse absorption feature evident in the 870-930 cm^{-1} region. With the exception of the rotational lines of the 927 cm^{-1} CO_2 band, the feature appears as a continuum at the observed 0.25 cm^{-1} resolution. Two other diffuse features, also consistent with the optical properties of H_2SO_4, appear to be present in the 990-1060 and 1125-1160 cm^{-1} regions.

VII. COMPARISON OF SPECTRAL THERMAL EMITTANCE MEASUREMENTS

In this section, a low spectral resolution comparison of all measurements of Venus obtained with reasonable calibration and atmospheric transmission corrections is presented, in order to determine the degree of variability in the thermal emittance spectrum. The spectral comparison is shown in Figure 12, with a chronological summary of the measurements given in Table I.

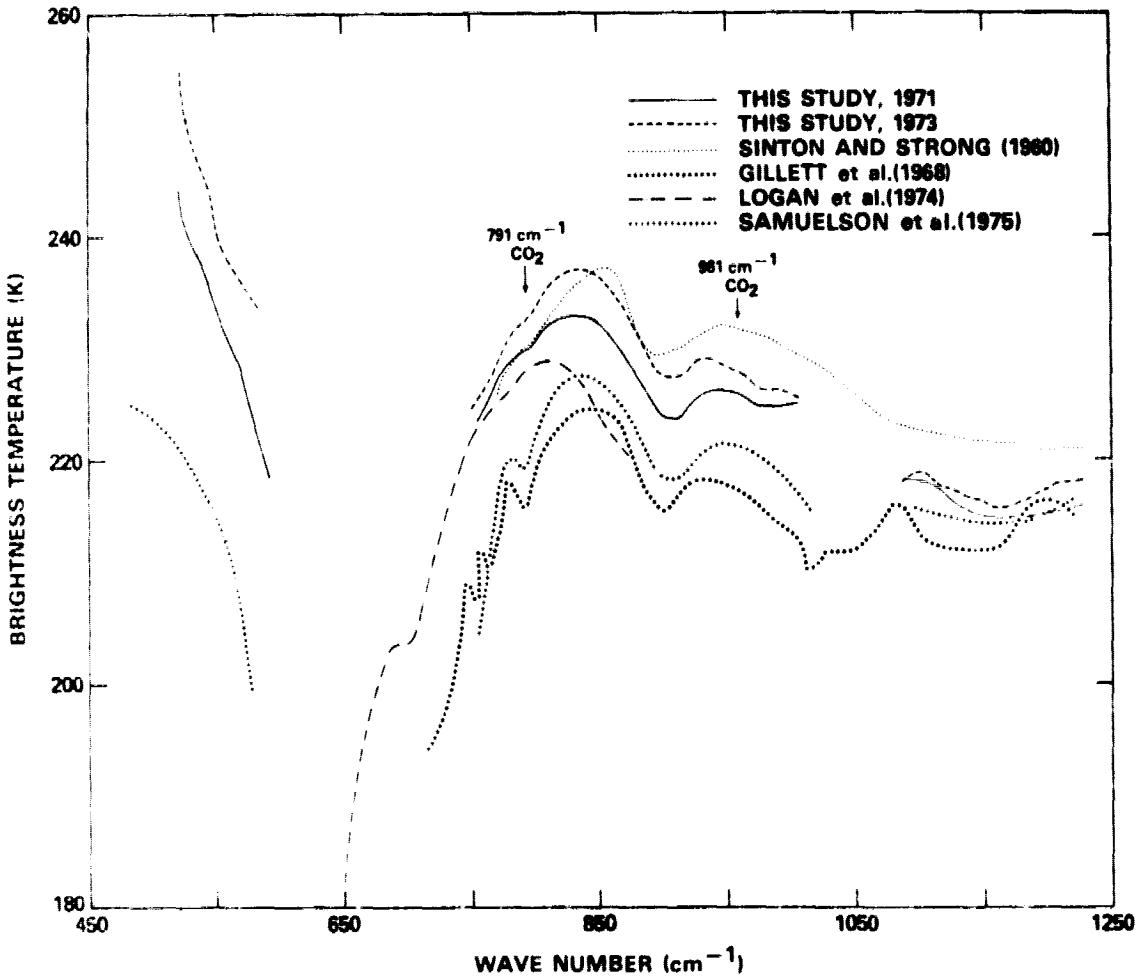

Figure 12. Comparsion of measurements of the thermal emittance spectrum of Venus at low spectral resolution. The observations of this study have been degraded to 20 cm^{-1}. A limb darkening correction has been applied to all measurements: thus the brightness temperature corresponds to a vertical intensity averaged over the field of view.

A literature review of both radiometric and spectrometric measurements of Venus has been presented by Cecil, et al., (1973). In Table I the maximum brightness temperature in the 750-1250 cm^{-1} range is represented by T_M, this maximum occurring in the 825 cm^{-1} region. All the measurements shown have been corrected for limb darkening; thus the brightness temperatures correspond to a vertical intensity averaged over the instrument field of view.

The first spectrum of the entire disk of Venus was obtained in 1953 by Sinton and Strong (1960) with a prism spectrometer. The resolving power was 28. A year later, a resolving power of 125 was obtained by the same authors with a grating spectrometer. Gillett et al. (1968) used a circular variable interference filter to measure the full disk spectrum in the 741-3571 cm^{-1} region with a resolving power of 50, corresponding to 20 cm^{-1} resolution at 1000 cm^{-1}. The interferometric observations of Hanel et al. (1968) were full disk measurements in the 750-1200 cm^{-1} range with about 1 cm^{-1} resolution. The brightness temperatures from these observations are considerably higher than those of other investigations, including the present one. Although temporal variations could be responsible for the high temperatures, it seems more probable that the 1968 spectrum contains a systematic error and, thus, these data are not included in Figure 12. Moroz et al. (1969) had difficulty correcting for atmospheric transmittance, and these spectra are not included in the comparison.

The emittance spectrum obtained in 1969 (Hanel et al., 1971; Samuelson et al., 1975), and the 1970-1971, and 1973 data discussed in this paper are presented at 20 cm^{-1} resolution, comparable to that of Gillett et al. (1968). Balloon-borne spectrometer measurements were obtained in the 625-2222 cm^{-1} region with resolving power of 25 by Logan et al., (1974). The decrease in terrestrial CO_2 absorption at float altitude (30km) allows the Venus emittance spectrum to be extended to the 660-750 cm^{-1} range. However, these measurements obviously have problems in either the spectral calibration or the data reduction because the 660-750 cm^{-1} region does not have the proper spectral character. The 667 cm^{-1} CO_2 band dominates the Venus emission in this region and the resulting spectrum should be nearly symmetrical with respect to the ν_2 Q-branch at 667 cm^{-1}. The spectrum of Ridgway (1975) is not included because an absolute calibration scale is not available.

All of the spectra exhibit a similar spectral character: The decrease in brightness temperature due to CO_2 absorption for the 500-800 cm^{-1} region, the diffuse absorption feature centered at 900 cm^{-1}, and relatively small thermal contrasts. The degree of variability in continuum brightness temperature is about 15-20K, small enough to be explained by physical changes, temporal or spati spatial, in the Venus stratosphere. Additionally, some or all of the spread may also be due to systematic calibration errors. Repreated high spatial resolution imaging with the same instrumentation, same observing site, and for the same

planet-sun configuration offer the best opportunity for establishing the real long-term variability of the Venus emergent radiances.

VIII. SUMMARY

Ground-based thermal emission spectra have been obtained for Venus during two observing sessions in 1970 and 1973. The measurements cover the 450-1250 cm^{-1} range with 0.25 cm^{-1} resolution. The general conclusions are:

(1) The high spectral resolution has allowed the Venus spectrum to be obtained in the 450-650 cm^{-1} region,

(2) The high spectral resolution has also allowed a number of weak CO_2 bands to be identified throughout the observed spectral range. Comparison with a synthetic model atmosphere indicates the observed thermal emission spectrum can be explained to first order with only gaseous CO_2 and an aqueous H_2SO_4 haze as sources of opacity. The absorbing properties of 75% aqueous solution H_2SO_4 haze at 250K gives general agreement throughout the observed spectral range. However, there are some regions of discrepancy due to the aerosol model requiring further investigation. One of these regions is around 450 cm^{-1} where the broad H_2SO_4 absorption feature does not seem to be present in the observed spectrum,

(3) No spectral evidence was found for gaseous H_2O or any other trace gas constituent,

(4) The observed brightness temperatures are in general agreement with previously measured temperatures to 15-20K. This degree of variation is understandable in terms of systematic errors or real "weather" type changes in the Venus stratosphere, and,

(5) General agreement has been found between synthetic and observed spectra of terrestrial transmittance and downward sky emittance.

ACKNOWLEDGMENTS

We thank B. J. Conrath for his constructive comments and M. Forman for useful discussions on Fourier Transform Theory.

REFERENCES

Cecil, T. E., Salisbury, J. W., Logan, L. M., and Hunt, G. R. (1973). Celestial infrared calibration sources in the 8-14 micrometer region: Venus and Jupiter. AFCRL-TR-73-0559, 5 September 1973.

Fjeldbo, G., Kliore, A., and Eshleman, V. R. (1971). The neutral atmosphere of Venus as studied with the Mariner 5 radio occultation experiment. Astron. J. 76, 123-140.

Gillett, F. C., Low, F. J., and Stein, W. A. (1968). Absolute spectrum of Venus from 2.8 to 14 microns. J. Atmos. Sci. 25, 594-595.

Hanel, R., Forman, M., Stambach, G., and Meilleur, T. (1968). Preliminary results of Venus observations between 8 and 13 microns. J. Atmos. Sci. 25, 586-593.

Hanel, R., Forman, M., Meilleur, T., Westcott, R., and Pritchard, J. (1969). A double beam interferometer for the middle infrared. Appl. Optics, 8, 2059-2065.

Hanel, R. A., Kunde, V. G., Meilleur, T., and Stambach, G. (1971). High spectral resolution interferometric planetary observation in the 7-25 μ region. In Planetary Atmospheres (IAU Symposium No. 40) (C. Sagan, T. C. Owen, and H. J. Smith, Eds.), pp. 44-47, Springer-Verlag, New York.

Herzberg G. (1945). In Molecular Spectra and Molecular Structure II. Infrared and Raman Spectra of Polyatomic Molecules. D. Van Nostrand Company, Inc., New York.

Kunde, V. G., and Maguire, W. C. (1974). Direct integration transmittance model. J. Quant. Spectrosc. Radiat. Transfer 14, 803-817.

Logan, L. M., Hunt, G. R., Long, D. A., and Dybwad, J. P. (1974). Absolute infrared radiance measurements of Venus and Jupiter. AFCRL-TR-74-0573, 15 November 1974.

McClatchey, R. A., Renn, R. W., Selby, J. E. A., Garing, J. S., and Volz, F. E. (1970). Optical properties of the atmosphere. ARCRL-70-0527, 22 September 1970.

McClatchey, R. A., Benedict, W. S., Clough, S. A., Burch, D. E., Calfee, R. F., Fox, K., Rothman, L. S., and Garing, J. S. (1973). AFCRL atmosphere absorption line parameters compilation. AFCRL-TR-73-0096, 26 January 1973.

Montgomery, C. G., Saari, J. M., Shorthill, R. W., and Six, Jr., N. F. (1966). Directional characteristics of lunar thermal emission. Technical Note R-213, Research Laboratories, Brown Engineering Co., Inc., Huntsville, Alabama.

Moroz, V. I., Davydov, V. D., and Zhegulev, V. S. (1969). Photometric and spectroscopic observations of planets in the 8-14 μ range. Soviet Astronomy — AJ 13, 101-109.

Pinkley, L. W., and Williams, D. (1976). The infrared optical constants of sulfuric acid at 250K. Preprint.

Pollack, J. B., Erickson, E. F., Goorvitch, D., Baldwin, B. J., Stecker, D. W., Witteborn, F. C., and Augason, G. C. (1976). A determination of the composition of the Venus clouds from aircraft observations in the near infrared. J. Atmos. Sci. 32, 1140-1150.

Ridgway, S. (1975). Private communication.

Samuelson, R. E., Hanel, R. A., Herath, L. W., Kunde, V. G., and Maguire, W. C. (1975). Venus cloud properties: Infrared opacity and mass mixing ratio. Icarus 25, 49-63.

Sinton, W. M., and Strong, J. (1960). Radiometric observations of Venus. Astrophys. J. 131, 470-490.

FIGURE CAPTIONS

Figure 1. Spectral transfer function to correct experimental wave number scale for finite field of view effects.

Figure 2. Telescope transmittance inferred from a comparison of measurements of the zenith sky through the telescope with similar measurements through an open port in the Coudé room. The line represents an approximate linear fit to the data points.

Figure 3. A, B. Atmospheric transmittance at 0.25 cm^{-1} resolution for the 400-650 and 650-900 cm^{-1} regions derived from observations of the moon. Numerous spectral lines are resolved for absorption bands of H_2O and CO_2. A synthetic comparison spectrum is also shown.

Figure 4. A, B. Atmospheric transmittance at 0.25 cm^{-1} resolution for the 900-1150 and 1150-1400 cm^{-1} regions derived from observations of the moon. Numerous spectral lines are resolved for absorption bands of CO_2, O_3, H_2O, N_2O and CH_4. A synthetic comparison spectrum is also shown.

Figure 5. Volume mixing ratios adopted for model atmosphere used to generate synthetic atmospheric transmittance.

Figure 6. A, B. Downward zenith sky emittance at 0.25 cm^{-1} resolution for the 400-650 and 650-900 cm^{-1} regions. Numerous spectral lines are resolved for absorption bands of H_2O and CO_2. A synthetic comparison spectrum is also shown.

Figure 7. A, B. Downward zenith sky emittance at 0.25 cm^{-1} resolution for the 900-1150 and 1150-1400 cm^{-1} regions. Numerous spectral lines are resolved from absorption bands of CO_2, O_3, H_2O, N_2O and CH_4. A synthetic comparison spectrum is also shown.

Figure 8. Venus thermal emittance spectrum in the 450-1250 cm^{-1} region at 0.25 cm^{-1} resolution obtained from McDonald Observatory in December 1970. A limb-darkening correction has been applied and the brightness temperatures correspond to the emergent radiance in the vertical. The integration time was ~ 52 minutes. The lines marked with an asterisk are residual terrestrial absorption lines which have not been completely compensated for by the correction techniques used. The residual effect is only important in the local region of the absorption line. The synthetic comparison spectrum has been displaced 20K vertically downward for clarity of presentation. The vertical arrows indicate this offset from the observed spectrum.

Figure 9. Same as Figure 8, except for 450-700 cm^{-1} region. Numerous CO_2 vibration-rotation absorption lines are evident, including the five distinct lines in the 450-500 cm^{-1} region. The lines in the 450-500 cm^{-1} range of the synthetic spectrum are due to Venusian H_2O. In the observed spectrum these lines have been blocked out by terrestrial H_2O.

Figure 10. Same as Figure 8, except for 750-1000 cm^{-1} region. Numerous CO_2 vibration-rotation absorption lines are evident. The broad absorption feature in the 900 cm^{-1} region is associated with the sulfuric acid haze. The lines in this feature are due to the 927 cm^{-1} CO_2 band.

Figure 11. Same as Figure 8, except for 1000-1250 cm^{-1} region. The only CO_2 band identified in the Venus spectrum in this region is at 1064 cm^{-1}.

Figure 12. Comparison of measurements of the thermal emittance spectrum of Venus at low spectral resolution. The observations of this study have been degraded to 20 cm^{-1}. A limb darkening correction has been applied to all measurements; thus the brightness temperature corresponds to a vertical intensity averaged over the instrument field of view.